Observation of two sequential pathways of $(CO_2)^{3+}$ dissociation by heavy-ion impact

S. Yan,[1] X. L. Zhu,[1] P. Zhang,[1] X. Ma,[1,*] W. T. Feng,[1] Y. Gao,[1] S. Xu,[1] Q. S. Zhao,[1] S. F. Zhang,[1] D. L. Guo,[1] D. M. Zhao,[1] R. T. Zhang,[1] Z. K. Huang,[1,2] H. B. Wang,[1,2] and X. J. Zhang[3]

[1]*Institute of Modern Physics, Chinese Academy of Sciences, Lanzhou 730000, China*

[2]*University of Chinese Academy of Sciences, Beijing 100049, China*

[3]*Henan University of Science and Technology, School of Physics and Engineering, Luoyang, 471023, China*

(Received 31 July 2016; published 21 September 2016)

An experimental investigation of the breakup of $(CO_2)^{3+}$ induced by Ne^{4+} ion impact at incident energies of 1.12 MeV was performed. By analyzing the momentum distributions and the kinetic energies of the three fragment ions, the nonsequential and sequential dissociation mechanisms are verified. In contrast to highly charged ion impact, two different sequential decay pathways were observed in the present experiment. One pathway originates from the primary cation $(CO_2)^{3+}$ populated into $^4\Sigma^+$ states by collision charge exchange and its daughter cation $(CO)^{2+}$ populated into the two excited states ($^3\Pi$ and $X\ ^1\Pi$) by the first fragmentation step, resulting in a lower KER peak. The other pathway originates from the primary cation $(CO_2)^{3+}$ locating at $^6\Pi$ state, and its daughter cation $(CO)^{2+}$ populated into the metastable excited states $^3\Pi$, $X\ ^1\Pi$, and $^3\Sigma^+$, leading to the higher KER peak. Our work is a breakup experiment of $(CO_2)^{3+}$ presenting the initial states of the parent cation $(CO_2)^{3+}$ and the metastable states of CO^{2+} ion simultaneously.

DOI: 10.1103/PhysRevA.94.032708

I. INTRODUCTION

Highly charged molecules or clusters are unstable and prefer to break into smaller fragments due to the Coulombic repulsion between the different ionic cores. The information of the dissociation dynamics will be imprinted in the final momentum distribution or the kinetic energy of the fragments. If all the charged fragments are measured in coincidence, the offline analysis of the behavior of the products will manifest the underlying dynamics leading bonds to breakup in the different pathways.

As a prototype system, the dissociation process $(CO_2)^{3+} \rightarrow C^+ + O^+ + O^+$ reveals two different decay mechanisms, namely, nonsequential and sequential fragmentation processes. For the nonsequential case, the primary $(CO_2)^{3+}$ cation breaks into C^+, O^+, and O^+ at the same time. While in the sequential process, the parent cation fragments into CO^{2+} and O^+ firstly; after several rotational periods, a dissociation of the daughter cation CO^{2+} takes place and results in two lighter ions. As the occurrence of the nonsequential and sequential process is eventually determined by the potential energy surfaces populated by the primary cations, the energy deposition from the projectile to the molecular-ion system becomes an essential parameter for understanding the complete decay pathways [1].

Fragmentation of CO_2 has been extensively studied in the past by the impact of highly charged ion (HCI) [1–4], x ray [5,6], electron [7–9], and intense lasers [10,11], and nonsequential and sequential dissociation processes are distinguished clearly. Most of the previous work focused only on identifying the existence of sequential dissociation. However, Ref. [7] not only demonstrated the existence of the sequential dissociation but also identified the initial states of the parent cation $(CO_2)^{3+}$, and Ref. [4] verified the metastable states of the dication CO^{2+} induced from the first breakup of $(CO_2)^{3+}$, $(CO_2)^{4+}$, and $(CO_2)^{5+}$ ions, respectively.

In the present study, we have chosen an intermediate velocity [1.4 atomic units (a.u.)] and a relatively lower charged projectile Ne^{4+}, which ensures the direct ionization, electron capture, and transfer ionization processes are all evoked. In this impact energy regime, numerous potential energy surfaces will be populated; thus a lot of sequential dissociation pathways stemming from different electronically exited states of parent cations might be opened. The coincidence measurement of the three fragment C^+, O^+, and O^+ ions provides the momentum distribution of each ion, the total KERs (sum of kinetic energies of the C^+, O^+, and O^+ ions), and the individual KERs associated to each breakup steps in the corresponding decay pathway. By combining the KERs and the momentum distributions of different ion pairs, two different sequential decay pathways are identified. Furthermore, the initial states of the parent cation $(CO_2)^{3+}$ and the metastable states of CO^{2+} are figured out.

II. EXPERIMENTAL METHOD

The experiment was carried out by utilizing a reaction microscope mounted at the 320-kV platform for multidisciplinary research with highly charged ions at the Institute of Modern Physics, Chinese Academy of Science [12–14]. Briefly, the Ne^{4+} ion beam is produced from the electron cyclotron resonance ion source and accelerated to 56 keV/u. After being collimated by two sets of slits and cleaned by two sets of electrostatic deflectors, the ion beam intersects with a cold supersonic CO_2 gas jet. The daughter ions induced from the dissociation processes following multiple ionization are extracted and accelerated toward the position-sensitive detector (PSD) by the electrostatic field. The scattered beam goes through one electrostatic deflector installed downstream of the interaction area and hits on another PSD that gives a trigger signal to the acquisition system. From the time of fight

*x.ma@impcas.ac.cn

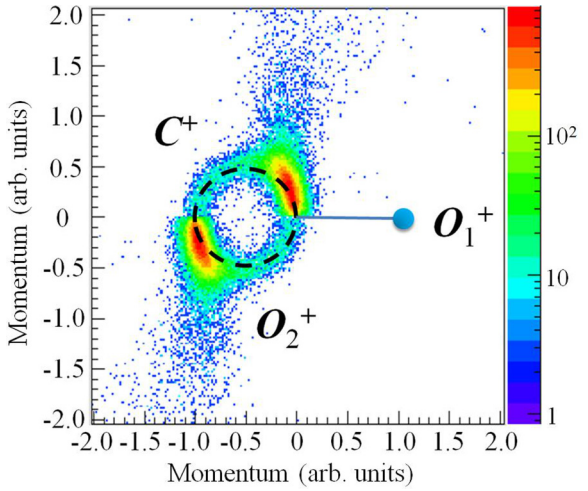

FIG. 1. Newton diagram for all events from three-body fragmentation of CO_2^{3+}.

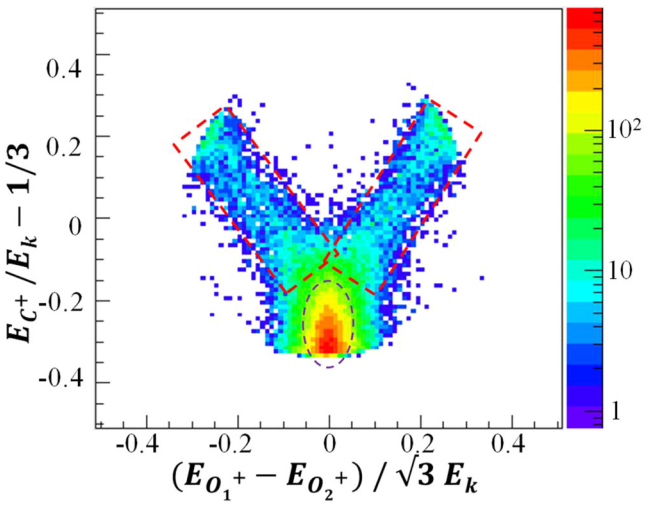

FIG. 2. Momentum correlation features for all events from three-body fragmentation of CO_2^{3+} in the Dalitz plot. The different areas labeled in the Dalitz plot correspond to different dissociation pathways. Black dashed oval: nonsequential dissociation. V-shaped area marked by the red dashed rectangle: sequential dissociation.

and the position information, momentum distributions of each ion are reconstructed.

III. RESULTS AND DISCUSSION

Under the present collision conditions, the interaction between the projectile and target is very fast (10^{-17}–10^{-16} s); the molecule has no time to adjust its initial geometry during the impact process, so the energy transfer between the projectile and the molecule can be reasonably considered as vertical transitions. Meanwhile, since the amount of deposited energy to the target CO_2 is random, the induced $(CO_2)^{3+}$ cation will be promoted into different electronically excited states. Afterwards, the structure geometry evolution along the corresponding potential energy surfaces begins and eventually induces fission of the parent cation into smaller fragments.

The Newton diagram of the three fragments of $(CO_2)^{3+}$ is shown in Fig. 1. In the center-of-mass frame, the momentum vector of the first arrived O^+ ion (O^+_{1st}) is represented as an arrow with its direction along the x axis and its length is set to 1. Then the momenta of the second detected O^+ ion (O^+_{2nd}) and the C^+ ion are normalized to that of the O^+_{1st} ion and are mapped in the lower and upper half plane of the diagram, respectively. This momentum-correlated plot reveals two apparent characteristics: one is the double-islands structure and the other one is the circle structure (marked by the black dashed circle). The islands structure indicates that the C^+ gains a very small amount of the kinetic energy during the breakup process, while the two O^+ ions are emitted back-to-back approximately, which means that the two C=O bonds break up synchronously, and the parent cation $(CO_2)^{3+}$ has the ground-state geometry of the CO_2 molecule. For the circle structure, the momentum sum of the O^+_{2nd} ion and the C^+ ion is constant and the center of the circle roughly locates at about 0.5 left side. These two features prove the existence of a sequential fragmentation process. The primary cation $(CO_2)^{3+}$ first breaks into the O^+_{1st} ion and the CO^{2+} ion. Then after some time, when the emitted O^+_{1st} ion moves far away from the CO^{2+} dication, the second fragmentation happens: the dication CO^{2+} breaks into the O^+_{2nd} ion and the C^+ ion.

The identification of nonsequential and sequential fragmentation processes can also be achieved by analyzing the Dalitz plot, which is a useful tool for understanding the three-body breakup dynamics [15,16]. In the two-dimensional plot, as shown in Fig. 2, the x and y coordinates are defined as follows:

$$x = \frac{E_{O^+_{1st}} - E_{O^+_{2nd}}}{\sqrt{3}E_k}, \tag{1}$$

$$y = \frac{E_{C^+}}{E_k} - \frac{1}{3}, \tag{2}$$

where $E_{O^+_{1st}}, E_{O^+_{2nd}}$ E_{C^+}, and E_k are the kinetic energies of the O^+_{1st} ion, the O^+_{2nd} ion, the C^+ ion, and the total energy of the three fragments, respectively. This probability-density plot represents the partitioning of momentum to all the fragment ions for three-body breakup processes in phase space, and each point of (x, y) reveals an identical momentum correlation among the three fragments induced from one breakup pathway.

There are two structures in the experimental Dalitz plot in Fig. 2: the bright area (marked by the black dashed oval) and the V-shaped area (marked by two red dashed rectangles). The events in the bright area indicate the nonsequential dissociation process, as the kinetic energy of the C^+ is very small and the two O^+ ions are emitted back-to-back, which corresponds to the double-islands structure in Fig. 1.

The three-body Dalitz plot can also be displayed in an equilateral triangle coordinate system; the normalized energy of the O^+_{1st} ion, the O^+_{2nd} ion, and the C^+ ion are represented by the perpendicular distances of the data point to the left edge, right edge, and bottom edge of the triangle, respectively. From this equilateral triangle coordinate, it can be concluded that the V-shaped area in Fig. 2 is attributed to the sequential dissociation. The right wing of the V-shaped area shows that the normalized energy of the O^+_{1st} ion is constant, e.g., the momentum correlation exists between the C^+ ion and the O^+_{2nd} ion. This phenomenon indicates that the O^+_{1st} ion is generated

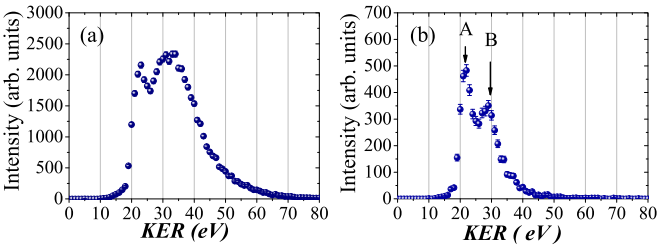

FIG. 3. Total KER distributions for three-body dissociation of CO_2^{3+}: (a) all events, not to distinguish sequential and nonsequential dissociation; and (b) the events corresponding to sequential dissociation.

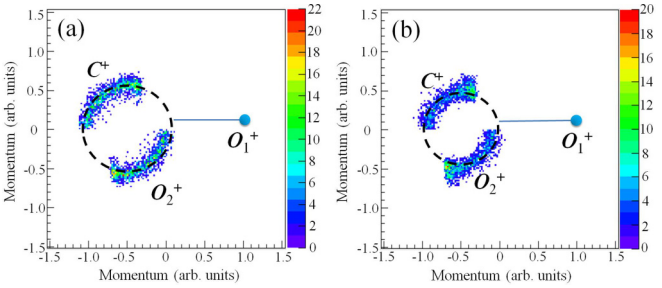

FIG. 4. Newton diagram for events corresponding to peak A (a) and peak B (b) in Fig. 3.

from the first fragmentation step, while the O^+_{2nd} ion arises from the second fragmentation step. On the contrary, for the left wing, the O^+_{1st} ion arises from the second fragmentation step, while the O^+_{2nd} ion is produced from the first fragmentation step.

The verification of the nonsequential and sequential dissociation of $(CO_2)^{3+}$ has been reported in previous works [1–10]. However, the total KER distribution in the present work shows a big difference to the KERs of HCI-molecule case [1]. Here, a broader peak is observed with its maximum located around 34 eV, besides the lower energy peak around 21 eV, as shown in Fig. 3(a). This peak tells us that the amount of energy deposited in the primary cation $(CO_2)^{3+}$ is larger compared with the case of Ar^{8+} impact. To form the parent cation $(CO_2)^{3+}$, the impact parameters of the $Ne^{4+} + CO_2$ collision should be smaller than that of the $Ar^{8+} + CO_2$ case, and the harder collision between Ne^{4+} and CO_2 results in more energy deposition into $(CO_2)^{3+}$, leaving the primary cation $(CO_2)^{3+}$ into more electronically excited states.

We reconstruct the KER distribution of sequential dissociation by picking up the events from the right wing of the V-shaped area in Fig. 2. As shown in Fig. 3(b), two significant peaks are observed, which indicates there are two pathways of sequential breakup. For convenience, the lower KER peak (around 21 eV is labeled as pathway *A*, while the higher KER peak (around 28.5 eV) is marked as pathway *B*.

In order to identify the initial states of $(CO_2)^{3+}$ corresponding to pathways *A* and *B*, we analyze the KER distribution in Fig. 3(b) with the help of the potential energy curves of Ref. [7]. We find that the KER for the dissociation via the $^4\Sigma^+$ state is estimated to be 21.8 eV, which is consistent with the peak value of pathway *A* in Fig. 3(b). Meanwhile, the dissociation through the repulsive state $^6\Pi$ results in the KER peaking at 29 eV, which well agrees with the peak value of pathway *B* in Fig. 3(b). Therefore, the $^4\Sigma^+$ state and $^6\Pi$ state may be attributed to the sequential dissociations of pathways *A* and *B*, respectively. Wang *et al.* [7] suggested that the states with stable potential wells tend to dissociate by a sequential process, and the repulsive states, which correspond to the total KER above 20 eV, prefer to relax through nonsequential dissociation. However, our result indicates that the repulsive states $^4\Sigma^+$ and $^6\Pi$ of $(CO_2)^{3+}$ ions may also decay via the sequential dissociation.

The events corresponding to pathways *A* and *B* are picked up to reconstruct their Newton diagrams, as shown in Figs. 4(a) and 4(b), respectively. Both of these two pathways exhibit a circle structure (marked by the black dashed circles); however, the diameter of the circle for pathway *A* is bigger than that of pathway *B*. This indicates that the relative energy partition in the second fragment step of pathway *A* is larger than that of pathway *B*. In order to understand the sequential fragmentation dynamics, the KER distribution of each breakup step will be reconstructed in the following.

The KER of the first fragmentation step can be written as $E_{O^+_{1st}} \times 44/28$, where the $E_{O^+_{1st}}$ is the kinetic energy of the $O_{1st}{}^+$ ion produced from the first fragmentation step. Correspondingly, the KER in the second step can be deduced as $E_{O^+_{2nd}} + E_{C^+} - \frac{(P_{C^+}+P_{O^+_{2nd}})^2}{2M_{CO}}$, where $E_{O^+_{2nd}}$ and E_{C^+} are the kinetic energy of the $O_{2nd}{}^+$ ion and C^+ ion produced from the second fragmentation step, P_{C^+} and $P_{O^+_{2nd}}$ are their corresponding momenta, and M_{CO} represents the mass of the daughter cation CO^{2+} produced in the first fragmentation step. The KER distributions of the first and the second fragmentation steps for both pathways *A* and *B* are presented in the horizontal panels of Fig. 5.

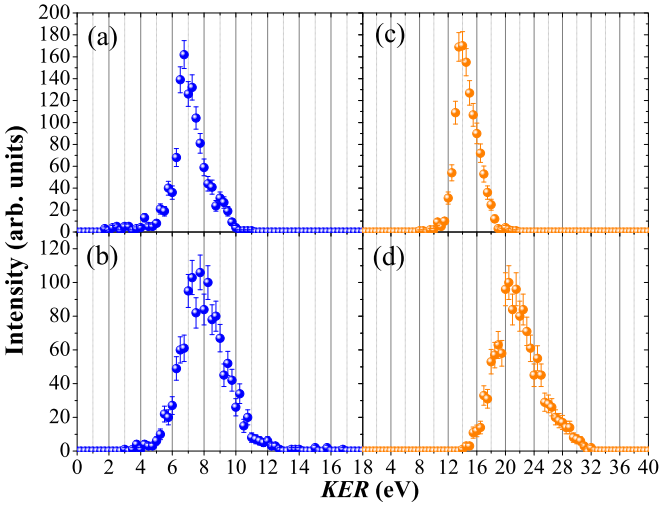

FIG. 5. The KER distributions corresponding to the first- and the second-step fragmentation for the events from pathway *A* and pathway *B*, respectively: (a).the second fragmentation step of pathway *A*; (b) the second fragmentation step of pathway *B*; (c) the first fragmentation step of pathway *A*; and (d) the first fragmentation step of pathway *B*.

For the second fragmentation step, as shown in Figs. 5(a) and 5(b), the peak value of KER distribution for pathway *A* is 6.7 eV, with the FWHM less than 2 eV. For pathway *B*, the peak value is slightly larger (around 7.5 eV), with the FWHM more than 3.5 eV. This phenomenon indicates that some metastable states of $(CO)^{2+}$ ion inducing pathway *A* may also contribute for the appearance of pathway *B*, but the number of states involved in pathway *A* is less than those in pathway *B*. For the first fragmentation step, as shown in Figs. 5(c) and 5(d), the difference of the KER distributions between pathways *A* and *B* is distinct: the peak value in pathway *A* is around 14 eV, while the one in pathway *B* is around 20.5 eV. This proves that, in the first steps, the dissociations of pathways *A* and *B* arise from different electronically excited states of $(CO_2)^{3+}$ ions. This agrees with the conclusion from Fig. 3(b).

Now, we turn to identify the metastable state of $(CO)^{2+}$ inducing the second fragmentation step. In principle, the metastable state of $(CO)^{2+}$ can be determined with the help of the KER exploration in the CO fragmentation experiment. In the past, numerous metastable states of $(CO)^{2+}$ were explored under various experimental conditions [17–20], while the high-resolution electron impact experiment [17] reveals the most probable candidate states: the KER distributions from the decays of $X\,^3\Pi$, $^1\Pi$, and $^3\Sigma^+$ states range from 5.6 to 6.6 eV, from 5.8 to 7.5 eV, and from 7.8 to 8.4 eV, respectively. By the comparison between our results in Figs. 5(a) and 5(b) with that from Ref. [17], it can be concluded that the metastable states of $(CO)^{2+}$ accounting for the second fragmentation step of pathway *A* are $X\,^3\Pi$ and $^1\Pi$ states. For pathway *B*, besides the contributions of $X\,^3\Pi$ and $^1\Pi$ states, the $^3\Sigma^+$ state also plays an important role.

IV. SUMMARY

In summary, the dissociation dynamics of $(CO_2)^{3+}$ induced by Ne^{4+} ion impact at incident energies 1.12 MeV has been explored. With the help of the Newton diagram and Dalitz plot, the nonsequential and sequential dissociation processes are clearly distinguished. By reconstructing the KER and the momentum of each fragment ion, two sequential decay pathways with different KER distributions were observed. The low KER pathway originates from the primary cation $(CO_2)^{3+}$ populated into $^4\Sigma^+$ states and its daughter cation $(CO)^{2+}$ populated into the two excited states ($^3\Pi$ and $X\,^1\Pi$) by the first fragmentation step. The high KER pathway originates from the primary cation $(CO_2)^{3+}$ locating at $^6\Pi$ state and its daughter cation $(CO)^{2+}$ populated into the metastable excited states $^3\Pi, X\,^1\Pi$, and $^3\Sigma^+$. Our work is a breakup experiment of $(CO_2)^{3+}$, presenting the initial states of the parent cation $(CO_2)^{3+}$ and the metastable states of CO^{2+} ion simultaneously.

ACKNOWLEDGMENT

This work is supported by the National Natural Science Foundation of China (Grants No. 11304325, No. U1332128, No. U1432118, and No. U1532129).

[1] N. Neumann, D. Hant, L. Ph. H. Schmidt, J. Titze, T. Jahnke, A. Czasch, M. S. Schöffler, K. Kreidi, O. Jagutzki, H. Schmidt-Böcking, and R. Dörner, Phys. Rev. Lett. **104**, 103201 (2010).

[2] M. R. Jana, P. N. Ghosh, B. Bapat, R. K. Kushawaha, K. Saha, I. Prajapati, and C. P. Safvan, Phys. Rev. A **84**, 062715 (2011); B. Siegmann, U. Werner, H. O. Lutz, and R. Mann, J. Phys. B: At. Mol. Opt. Phys. **35**, 3755 (2002).

[3] L. Adoui, T. Muranaka, M. Tarisien, S. Legendre, G. Laurent, A. Cassimi, J.-Y. Chesnel, X. Fléchard, F. Frémont, B. Gervais, E. Giglio, and D. Hennecart, Nucl. Instrum. Meth. B **245**, 94 (2006).

[4] A. Khan, L. C. Tribedi, and D. Misra, Phys. Rev. A **92**, 030701 (2015).

[5] R. Guillemin, P. Decleva, M. Stener, C. Bomme, T. Marin, L. Journel, T. Marchenko, R. K. Kushawaha, K. Jänkälä, N. Trcera, K. P. Bowen, D. W. Lindle, M. N. Piancastelli, and M. Simon, Nat. Commun. **6**, 6166 (2015).

[6] R. K. Singh, G. S. Lodha, V. Sharma, I. A. Prajapati, K. P. Subramanian, and B. Bapat, Phys. Rev. A **74**, 022708 (2006).

[7] E. Wang, X. Shan, Z. Shen, M. Gong, Y. Tang, Y. Pan, K.-C. Lau, and X. Chen, Phys. Rev. A **91**, 052711 (2015).

[8] P. Bhatt, R. Singh, N. Yadav, and R. Shanker, Phys. Rev. A **85**, 042707 (2012).

[9] X. Wang, Y. Zhang, D. Lu, G. C. Lu, B. Wei, B. H. Zhang, Y. J. Tang, R. Hutton, and Y. Zou, Phys. Rev. A **90**, 062705 (2014).

[10] C. Wu, C. Wu, D. Song, H. Su, Y. Yang, Z. Wu, X. Liu, H. Liu, M. Li, Y. Deng, Y. Liu, L.-Y. Peng, H. Jiang, and Q. Gong, Phys. Rev. Lett. **110**, 103601 (2013); C. Wu, C. Wu, Y. Fan, X. Xie, P. Wang, Y. Deng, Y. Liu, and Q. Gong, J. Chem. Phys. **142**, 124303 (2015).

[11] A. Hishikawa, A. Iwamae, and K. Yamanouchi, Phys. Rev. Lett. **83**, 1127 (1999).

[12] X. Ma, R. T. Zhang, S. F. Zhang, X. L. Zhu, W. T. Feng, D. L. Guo, B. Li, H. P. Liu, C. Y. Li, J. G. Wang, S. C. Yan, P. J. Zhang, and Q. Wang, Phys. Rev. A **83**, 052707 (2011).

[13] S. Yan, P. Zhang, X. Ma, S. Xu, S. X. Tian, B. Li, X. L. Zhu, W. T. Feng, and D. M. Zhao, Phys. Rev. A **89**, 062707 (2014).

[14] S. Yan, P. Zhang, X. Ma, S. Xu, B. Li, X. L. Zhu, W. T. Feng, S. F. Zhang, D. M. Zhao, R. T. Zhang, D. L. Guo, and H. P. Liu, Phys. Rev. A **88**, 042712 (2013).

[15] R. Dalitz, London Edinburgh Dubl. Philos. Mag. J. Sci. **44**, 1068 (1953).

[16] M. Schulz, R. Moshammer, W. Schmitt, H. Kollmus, R. Mann, S. Hagmann, R. E. Olson, and J. Ullrich, Phys. Rev. A **61**, 022703 (2000).

[17] M. Lundqvist, P. Baltzer, D. Edvardsson, L. Karlsson, and B. Wannberg, Phys. Rev. Lett. **75**, 1058 (1995).

[18] J. H. D. Eland, Chem. Phys. **294**, 171 (2003).

[19] J. McKenna, A. M. Sayler, F. Anis, N. G. Johnson, B. Gaire, U. Lev, M. A. Zohrabi, K. D. Carnes, B. D. Esry, and I. Ben-Itzhak, Phys. Rev. A **81**, 061401 (2010).

[20] T. Šedivcová, P. R. Žd'ánská, V. Špirko, and J. Fišer, J. Chem. Phys. **124**, 214303 (2006).